Enhanced neuronal excitability in the absence of neurodegeneration induces cerebellar ataxia

See the related Commentary beginning on page 505.

Vikram G. Shakkottai,[1] Chin-hua Chou,[1] Salvatore Oddo,[2] Claudia A. Sailer,[3] Hans-Günther Knaus,[3] George A. Gutman,[4] Michael E. Barish,[5] Frank M. LaFerla,[2] and K. George Chandy[1]

[1]Department of Physiology and Biophysics, and
[2]Department of Neurobiology and Behavior, University of California Irvine, Irvine, California, USA
[3]University of Innsbruck, Department of Biochemical Pharmacology, Innsbruck, Austria
[4]Department of Microbiology and Molecular Genetics, University of California Irvine, Irvine, California, USA
[5]Division of Neurosciences, Beckman Research Institute of the City of Hope, Duarte, California, USA

Cerebellar ataxia, a devastating neurological disease, may be initiated by hyperexcitability of deep cerebellar nuclei (DCN) secondary to loss of inhibitory input from Purkinje neurons that frequently degenerate in this disease. This mechanism predicts that intrinsic DCN hyperexcitability would cause ataxia in the absence of upstream Purkinje degeneration. We report the generation of a transgenic (Tg) model that supports this mechanism of disease initiation. Small-conductance calcium-activated potassium (SK) channels, regulators of firing frequency, were silenced in the CNS of Tg mice with the dominant-inhibitory construct SK3-1B-GFP. Transgene expression was restricted to the DCN within the cerebellum and was detectable beginning on postnatal day 10, concomitant with the onset of cerebellar ataxia. Neurodegeneration was not evident up to the sixth month of age. Recordings from Tg DCN neurons revealed loss of the apamin-sensitive after-hyperpolarization current (I_{AHP}) and increased spontaneous firing through SK channel suppression, indicative of DCN hyperexcitability. Spike duration and other electrogenic conductance were unaffected. Thus, a purely electrical alteration is sufficient to cause cerebellar ataxia, and SK openers such as the neuroprotective agent riluzole may reduce neuronal hyperexcitability and have therapeutic value. This dominant-inhibitory strategy may help define the in vivo role of SK channels in other neuronal pathways.

J. Clin. Invest. **113**:582–590 (2004). doi:10.1172/JCI200420216.

Introduction

Cerebellar ataxia, a disease characterized by incoordination, instability of posture, gait abnormalities, and intention tremor, has many molecular causes (1–5). Hereditary cerebellar ataxias are slowly progressive, and the genes responsible for 50–60% of hereditary ataxias have been identified, but the molecular basis for the others, as well as for sporadic ataxias, remains elusive (1–5). Cerebellar cortical degeneration is a hallmark of this disease, and, irrespective of the nature of the cerebellar cortical defect, degeneration results in altered Purkinje neuron output (3). Since Purkinje neurons constitute the sole output of the cerebellar cortex (6) and they primarily project inhibitory signals to the deep cerebellar nuclei (DCN) (3, 7), impaired Purkinje neuronal function would be expected to enhance DCN hyperexcitability. DCN neurons fire spontaneously in the absence of synaptic input from Purkinje neurons (7, 8), and modulation of the DCN firing response by Purkinje input is believed to be responsible for coordination of movement. DCN neurons in turn project to motor centers in the nervous system, and enhanced DCN excitability might affect motor performance at multiple levels.

A plausible mechanism for the initiation of cerebellar ataxia may therefore involve increased excitability of the DCN secondary to loss of inhibitory Purkinje input. If this mechanism were the cause, intrinsic DCN hyperexcitability would be predicted to cause cerebellar ataxia without upstream cerebellar cortical degeneration. All existing animal models of cerebellar ataxia exhibit cerebellar cortical degeneration (3), however, making it difficult to test this prediction. Furthermore, the electrical status of the DCN in these models cannot be determined because slice preparations sever the connections between Purkinje neurons and the DCN (9), precluding analysis of the DCN's

Received for publication October 6, 2003, and accepted in revised form November 25, 2003.

Address correspondence to: K. George Chandy, Department of Physiology and Biophysics, University of California Irvine, Joan Irvine Smith Hall, Room 291, Irvine, California 92697, USA. Phone: (949) 824-6370; Fax: (949) 824-3143; E-mail: gchandy@uci.edu.

Conflict of interest: The authors have declared that no conflict of interest exists.

Nonstandard abbreviations used: deep cerebellar nuclei (DCN); transgenic (Tg); small-conductance calcium-activated potassium (SK); apamin-sensitive after-hyperpolarization current (I_{AHP}); calmodulin (CaM); glial fibrillary acidic protein (GFAP); artificial CSF (ACSF).

electrical status in the presence of impaired Purkinje inhibitory input. The lack of a DCN-specific promoter has further precluded direct testing of this hypothesis in transgenic (Tg) models.

One approach to enhance the intrinsic excitability of the DCN is to selectively block small-conductance calcium-activated potassium (SK) channels that underlie the apamin-sensitive component of the after-hyperpolarization current (I_{AHP}) and regulate firing frequency (7, 10). SK channels are products of the *SK1, SK2,* and *SK3* genes and are gated in a Ca^{2+}-calmodulin-dependent (CaM-dependent) manner (11). We recently described a novel SK3 transcript, SK3-1B, that exhibits specific SK channel family-wide negative dominance when expressed in heterologous expression systems (12). SK3-1B was used to silence SK channels in the brains of Tg mice. To facilitate detection of the transgene product, we tagged SK3-1B in-frame at the C terminus with GFP without affecting function (12). SK3-1B-GFP was expressed under the control of the neuron-specific mouse Thy1.2-SX promoter, which is transcriptionally active in the CNS throughout adult life, especially in the DCN, and has been used successfully in other Tg constructs (13–15). Transgene expression driven by this promoter varies depending on the founder Tg line (14, 15), and we were able to identify two lines with transgene expression in the DCN but not elsewhere in the cerebellum. These mice developed severe cerebellar ataxia accompanied by increased firing frequency of DCN neurons in the absence of neurodegeneration. This Tg model supports the notion that DCN hyperexcitability may be an important step in the initiation of cerebellar ataxia and sheds light on the in vivo role of SK channels in regulating DCN firing frequency.

Methods

Generating and characterizing Tg mice. The murine Thy1.2-SX promoter construct (13) contains the neuron-specific Thy1.2 promoter and exons I_a, I_b, II (with a deletion just upstream of the AUG and an engineered multiple-cloning site), and IV (with a 5′ partial deletion). The SK3-1B-GFP fragment (12) was released from the EGFP-N1 vector as a *XhoI*/*XbaI* fragment and cloned into the *SalI*/*NheI* sites of the Thy1.2-SX construct. Vector sequences were removed by digestion with *EcoRI*/*PvuI,* and the 8.7-kb Thy1.2-SX-SK3-1B-GFP was isolated. Tg mice were generated by pronuclear microinjection in CB6F1 mice (hybrid of C57BL/6J × BALB/c) because of their known "hybrid vigor" and proclivity to produce large litters. Tg mice were identified using PCR with a GFP 5′ primer and a 3′ primer in Thy1.2 and by probing Southern blots with a 5.4-kb *BamHI* fragment of the linearized Tg (final stringency wash in Southern blot 70°C 0.1% SDS and 0.1× SSC). Of the 13 founders, the D2 and D11 founders were selected because of their prominent phenotype, robust Tg expression in the DCN but not elsewhere in the cerebellum, and because they bred normally with CB6F1 mice. These founders were mated with normal CB6F1 mice to obtain F_1 litters and were maintained hemizygous for the transgene so that each litter contained age-matched non-Tg controls. The penetrance of the phenotype in the D2 and D11 offspring was 100%.

For immunoblotting, lysates (in 2% SDS) prepared from one-half of the brains of Tg mice or non-Tg littermates were electrophoresed, blotted, and probed with anti-GFP (1:1,000; Roche Diagnostics Corp., Indianapolis, Indiana, USA.) or anti–β actin Ab's (1:5,000; Sigma-Aldrich, St. Louis, Missouri, USA), followed by HRP-labeled goat anti-mouse IgG (Jackson ImmunoResearch Laboratories Inc., West Grove, Pennsylvania, USA) and chemiluminescent detection (Pierce Chemical Co., Rockford, Illinois, USA).

Motor tasks. All experiments with animals were performed under the aegis of animal protocols approved by the Institutional Animal Care and Use Committees at University of California, Irvine, and Beckman Research Center at City of Hope in centers accredited by the Association for Assessment and Accreditation of Laboratory Animal Care. Mice were tested for motor function at 8, 12, and 16 weeks of age, following 2 weeks of handling to make them comfortable with the investigator (16, 17). For the hanging wire task, mice were placed on a standard wire cage lid, which was turned upside down, and the latency to fall-off was measured. A 120-second cut-off time was used. The ability to maintain balance on the constant-speed rotarod (Accuscan Instruments Inc., Columbus, Ohio, USA) at 5 rpm was measured by the latency to fall-off. Each trial was 180-seconds long, and trials were repeated six times per day on five consecutive days. In other experiments, mice were placed on a stationary rod with eight trials per mouse, each trial lasting 180 seconds. A total of 9–19 Tg and non-Tg littermates were used for the constant-speed and stationary rod experiments. Gait ataxia was quantified from the footprint pattern of mice (16, 17). Hind forefoot discordance was measured as the distance between the hindfoot and forefoot pads in each step for three sequential steps. Stride length was measured between the central pads of the two consecutive prints on each side. A total of 6–14 Tg and non-Tg littermates were analyzed in each experiment. Statistical analysis was done by one-way ANOVA.

Immunohistochemistry. Brain or spinal cord samples were embedded in paraffin and 6-μm sections were mounted on silane-coated slides. Slides were dewaxed, rehydrated, and stained with appropriate histological stains. For immunohistochemistry, sections were stained with appropriate primary and secondary Ab's. Ab's specific for SK1, SK2, and SK3 (18) were used at dilutions of 1:50, 1:2,000, and 1:1,000, respectively. The anti-SK3 Ab detects mouse SK3 but not SK3-1B-GFP. Ab's specific for GFP (Molecular Probes Inc., Eugene, Oregon, USA) and glial fibrillary acidic protein (GFAP) (DAKO Corp., Carpinteria,

California, USA) were used at dilutions of 1:500 and 1:3,000, respectively. Biotinylated goat anti-rabbit IgG was purchased from Jackson ImmunoResearch Laboratories Inc. The sections were developed with diaminobenzidine substrate using avidin-biotin HRP (Vector Laboratories, Burlingame, California, USA). Antigen retrieval with trypsin was performed for immunostaining with anti-GFAP, anti-SK2, and anti-SK3. Microwave treatment was used for antigen retrieval for anti-SK1.

Brain sections from 14 Tg mice and 14 controls aged 10–180 days were analyzed for Tg expression; sections from 20 Tg mice and 20 controls were stained with H&E, and sections from five Tg mice and four controls were stained for GFAP. Seven Tg and five control brain sections were stained with Fluorojade (19) solution (HistoChem Inc., Jefferson, Arkansas, USA) for 30 minutes, followed by counterstaining with DAPI.

Cerebellar slice recording. Whole-cell recordings were conducted on cerebellar slice preparations from mice aged 12–13 days, when Tg expression is detectable by immunostaining and behavioral changes are evident. DCN neurons in older mice could not be studied due to myelination. Mouse brains (removed after halothane anesthesia) were chilled in ice-cold dissection solution containing (in mM): 87 NaCl, 2.5 KCl, 25 $NaHCO_3$, 1 NaH_2PO_4, 0.5 $CaCl_2$, 7 $MgCl_2$, 75 sucrose, and 10 glucose, and bubbled with carbogen (5% CO_2/95% O_2). Coronal cerebellar slices (250 μm) were cut with a Vibratome and transferred to 35.5°C artificial CSF (ACSF) for approximately 1 hour before reducing the bath to ambient temperature. ACSF contained (in mM): 125 NaCl, 2.5 KCl, 26 $NaHCO_3$, 1.25 NaH_2PO_4, 2 $CaCl_2$, 2 $MgCl_2$, and 20 glucose, and was bubbled with carbogen (5% CO_2/95% O_2). In some experiments, $CaCl_2$ was replaced with equimolar $BaCl_2$, or 200 μM Cd^{2+} was added to the bath solution. Patch pipettes with a resistance of 2.5–4.0 MΩ were pulled from borosilicate glass capillaries (TW150F; WPI, Sarasota, Florida, USA). DCN neurons were visualized with differential interference contrast optics on an Olympus BX-50WI upright microscope. Whole-cell recordings were made at room temperature between 1 and 4–5 hours after slice preparation using an Axopatch 200B amplifier, Digidata 1200 interface, and pClamp-9 software (Axon Instruments Inc., Union City, California, USA).

I_{AHP} was investigated under a voltage clamp with an established protocol for SK channels (10) and was initiated by application of a 50-mV depolarizing step from a nominal holding potential of –50 mV to induce Ca^{2+} entry through voltage-gated Ca^{2+} channels. The amplitude of apamin-resistant K^+ conductance was measured at the end of the depolarizing step used to elicit the I_{AHP}. The pipette solution (10) contained (in mM): 135 $KMeSO_4$, 8 NaCl, 10 HEPES, 2 Mg_2ATP, and 0.3 Na_3GTP. I_{AHP} amplitude was estimated as the current amplitude 45 ms after repolarization (the time of peak I_{AHP}). Current and voltage traces were sampled at 10 kHz and analyzed using Clampfit 9 and Origin 7 (OriginLab Corp., Northhampton, Massachusetts, USA). A junction potential of 10 mV was compensated in voltage traces. Capacity transients were compensated by eye using the Axopatch amplifier. Series resistance was monitored but not compensated, and cells were rejected if series resistance exceeded 25 MΩ.

To record Ca^{2+} currents (20), the pipette solution contained (in mM): 120 CsCl, 20 tetraethyl ammonium, 2 $MgCl_2$, 3 Na_2ATP, 0.2 Na_3GTP, 5 EGTA, and 10 HEPES. Ca^{2+} currents were elicited with 1-second depolarizing voltage steps to –20 mV from a holding

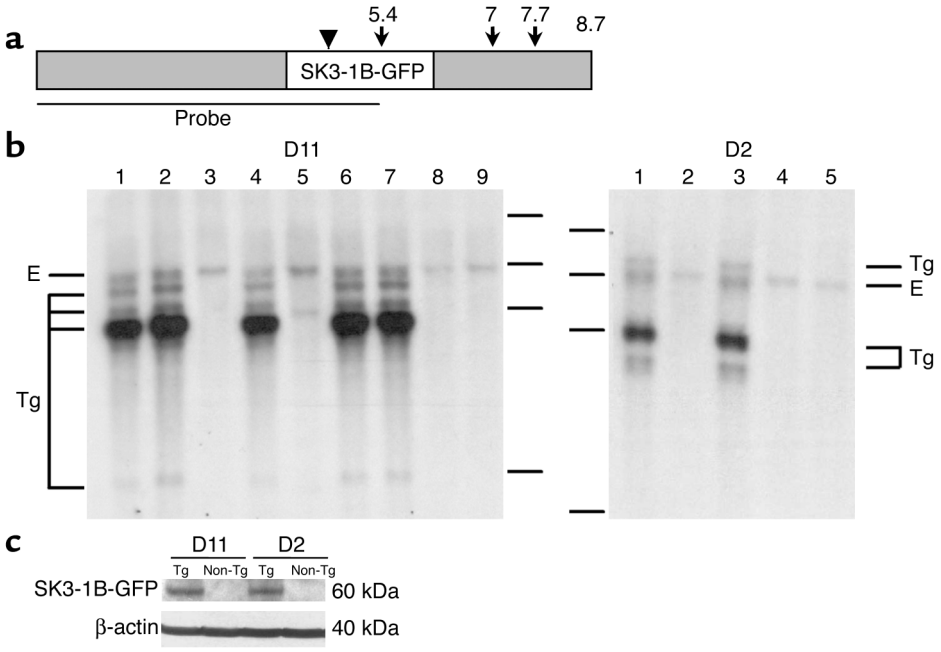

Figure 1
Characterization of SK3-1B-GFP Tg mice. (**a**) Locations of Thy1.2 (gray) and SK3-1B-GFP in transgene cassette with *BamHI* restriction sites indicated by arrows (numbers above arrows represent kilobases from 5′ end of cassette). Initiation codon is indicated by inverted arrowhead. A 5.4-kb probe for Southern blot analysis is indicated by line below cassette. (**b**) *BamHI* digests of tail DNA in D11 and D2. Molecular weights (in kilobases: 23, 9.4, 6.6, 2.3). A 9.2-kb endogenous band (E) seen in all lanes. Tg-specific bands (Tg) seen in D11 lanes 1, 2, 4, 6, 7 and in D2 lanes 1 and 3. (**c**) Western blot analysis of brain extracts probed with anti-GFP and anti–β-actin Ab's.

potential of –70 mV delivered every 30 seconds. Peak current was measured at the beginning of the voltage step, and Ca^{2+} channel inactivation was calculated as the fraction of current lost from the peak to the time of repolarization.

Results

Derivation of Tg mice. Of 82 progeny, 13 carried the transgene as determined by PCR and Southern blot analysis. Of these 13 founders, 7 developed cerebellar ataxia (see Supplementary videos, http://www.jci.org/cgi/content/full/113/4/582/DC1). Two independent lines (D2 and D11) selected for further study expressed the transgene in the DCN, but not other cerebellar neurons. These were maintained as hemizygous lines for the transgene so that each litter contained non-Tg offspring to serve as age-matched controls. Analysis of two lines ensured that the phenotype was not due to an integration artifact.

The transgene cassette is shown in Figure 1a with *BamHI* restriction sites indicated by arrows and the initiation codon by an arrowhead. *BamHI* digests of tail DNA from F_1 mice of the D11 and D2 lines were hybridized with the 5.4-kb probe defined by the solid line shown below the cassette. The Southern blot in Figure 1b revealed Tg-specific bands in D11 Tg mice (7.4 kb, 6.8 kb, 6.4 kb, and 2.3 kb in lanes 1, 2, 4, 6, 7) and D2 Tg mice (10.1 kb, 6.4 kb, 4.9 kb in lanes 10 and 12). An endogenous 9.2-kb band was seen in both Tg and non-Tg lanes.

In the transgene construct, translation initiates at position 789 in SK3-1B to generate a fusion protein of approximately 60 kDa (33 kDa SK3-1B and 27 kDa GFP). Western blots revealed comparable steady-state levels of the 60-kDa Tg product (Figure 1c) in both Tg lines.

Severe cerebellar ataxia exhibited by the mice. Tg mice gained weight normally (Figure 2) and exhibited activity-dependent intention tremor that disappeared at rest, characteristic of cerebellar ataxia. Ataxia was first evident on postnatal day 11 and progressively worsened until week 3. Four behavioral tests — hanging wire, stationary rod, rotarod, and gait analysis — were used to quantitatively evaluate cerebellar ataxia in mice between 8–16 weeks of age. Younger mice could not perform the motor performance tasks. Tg mice fell off the stationary rod with a significantly shortened latency than did non-Tg littermates, indicating impaired ability to maintain equilibrium at rest ($P < 0.001$, Figure 2a); balance improved between 8 and 12 weeks, with no further improvement at 16 weeks. On the constant-speed rotarod (5 rpm), Tg mice fell off more rapidly than non-Tg controls over five consecutive days of testing (Figure 2b), demonstrating significantly defective motor learning and equilibrium at motion; their ability to balance on the rotarod did not change between 8 and 16 weeks. Tg mice performed poorly on the hanging wire task that measures balance and grip strength ($P < 0.001$, Figure 2c). Gait ataxia was obvious by day 23 (see Supplementary videos, http://www.jci.org/cgi/content/full/113/4/582/DC1). We quantified gait ataxia by measuring the hindfoot-forefoot discordance on inked foot imprints on paper. In normal mice the hindfoot and forefoot placements nearly superimpose, whereas in ataxic mice there is discordance in their placement. Hindfoot-forefoot discordance was statistically significant by 12 weeks in D11 and 16 weeks in D2 Tg mice compared with the corresponding non-Tg littermates (Figure 2d). The stride length of Tg mice was comparable to controls (not shown). This combination of intention tremor, postural instability, incoordination, gait ataxia in the absence of postural abnormalities, overt muscle wasting, rigidity, and sensory deficits closely resembles cerebellar ataxia (1–5). This spectrum of motor deficits strongly suggests cerebellar dysfunction as the major cause of the Tg phenotype.

Transgene expression is detected only in the DCN within the cerebellum and is not accompanied by neurodegeneration. The pattern of transgene expression was analyzed by immunohistochemistry for GFP in mouse brain sections. We focused on the cerebellum since the ataxic phenotype pointed strongly to a cerebellar origin. Transgene expression within the cerebellum was detected exclusively within large DCN neurons that have been previously shown to be glutamatergic projection neurons (21). Expression was detected as early as postnatal day 10, preceding by a day the onset of cerebellar ataxia (Figure 3a). No expression was detected in the cerebellar cortex.

Brains from Tg and non-Tg mice aged 10–180 days of age were sectioned and examined for signs of neurode-

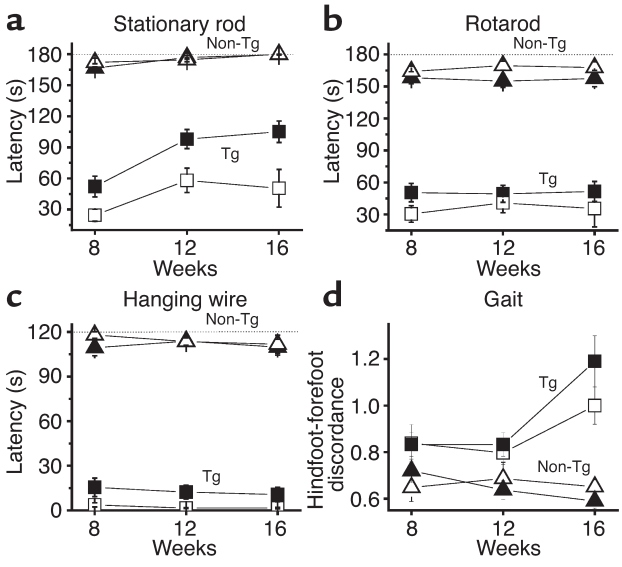

Figure 2
Performance on motor tasks. (**a**) Stationary rod; (**b**) rotarod; (**c**) hanging wire task; (**d**) hindfoot-forefoot discordance (n = 7–14 Tg; 6–12 non-Tg). D11 non-Tg (filled triangles), D2 non-Tg (open triangles), D11 Tg (closed squares), D2 Tg (open squares) (n = 10–19 Tg; 9–18 non-Tg). Body weights: 4 weeks old: Tg 18.5 ± 0.9 g, non-Tg 17.6 ± 0.8 g; 12 weeks old: Tg 26.9 ±1.3 g, non-Tg 25.7 ± 1.2 g. Error bars = SEM.

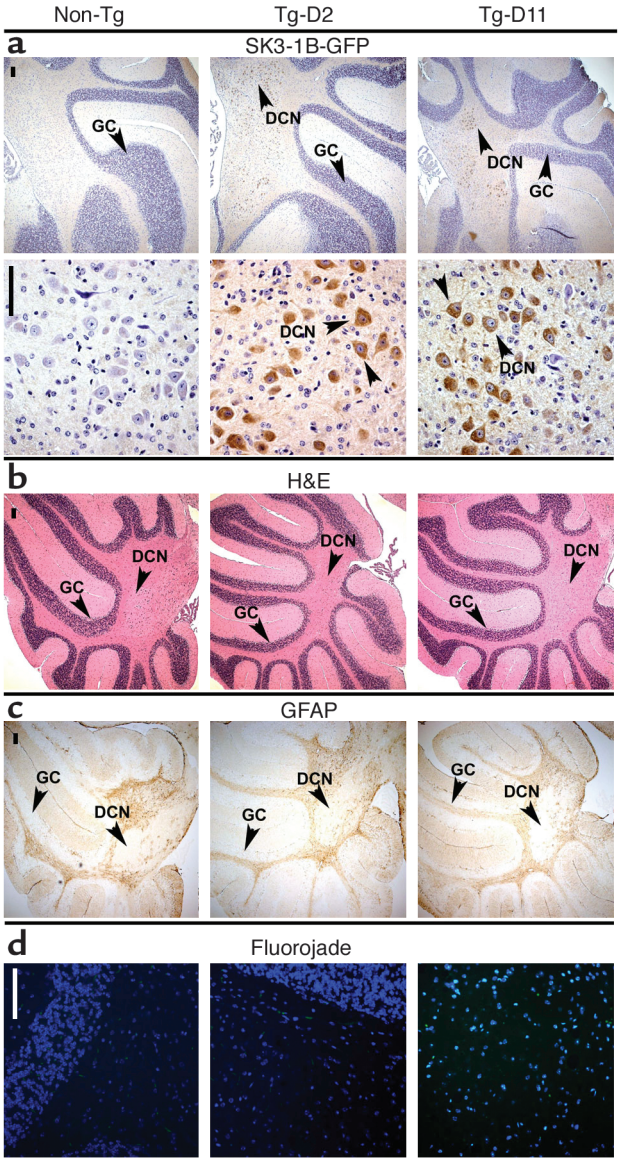

Figure 3
SK3-1B-GFP is expressed in DCN neurons that express SK1 and SK2 and does not cause neurodegeneration. (**a**) Immunoperoxidase staining for GFP with hematoxylin counterstaining revealed transgene expression in the large neurons in the DCN (brown cells indicated by arrowheads in middle and right panels) but not in the cerebellar cortex (indicated by arrowhead pointing to granule cell layer in cerebellar cortex) shown at 5 weeks of age. GC, granule cell layer. (**b**) In sections from 12-week-old mice stained with H&E, cerebellar architecture appears normal. (**c**) There is no evidence of reactive gliosis in Tg cerebellar sections immunostained for GFAP at 12 weeks of age. (**d**) Fluorojade shows no staining (blue DAPI counterstained cells with no green fluorojade-positive cells) in cerebellar sections from mice aged 12 weeks. Scale bars = 100 μm.

generation. H&E-stained sections of Tg mice did not show overt alterations in cerebellar architecture up to 6 months of age (Figure 3b), and immunostaining for GFAP failed to identify reactive gliosis (Figure 3c). Furthermore, Fluorojade (19), a marker for degenerating neurons, did not stain Tg brain sections (Figure 3d), corroborating the lack of significant histopathological effect of transgene expression. Neurodegeneration was also not evident by H&E (Figure 4, left), GFAP, and Fluorojade staining (not shown) in any other region of the CNS, including the cortex, midbrain, brain stem, and spinal cord up to 6 months of age.

The transgene product was also detected in neocortical layer V neurons, brain stem nuclei (red, pontine, hypoglossal, gigantocellular), and ventral horn neurons of the spinal cord (Figure 4, right). We assessed transgene expression in the D2 and D11 lines and other founder mice we had available and compared these levels with disease severity. Expression levels are tabulated in Table 1 with examples of stained sections demonstrating the grading scheme in Figure 5. Disease severity correlated well with transgene expression levels in the DCN; it was highest in mice with severe ataxia, low in mice with mild ataxia, and absent in the B3 and A1 founders that did not develop disease (Table 1). No expression was seen in the cerebellar cortex in the brain of any mouse examined. Transgene levels in other nuclei did not correspond with severity of cerebellar ataxia. Transgene expression in the motor strip was generally weaker than in the DCN and was low in the D2 line with severe ataxia, absent in the A2 and F4 founders with mild ataxia, and present in the B3 founder with no ataxia (Table 1). A lack of correspondence was also observed between transgene expression in the pontine nuclei and disease severity, since the F5 and D9 founders with severe ataxia had intermediate levels of the transgene, and no expression was seen in A2 and F4 founders with mild ataxia (Table 1). In the case of the red nucleus, robust transgene expression was seen in the A2 founder that had only mild ataxia, and low expression was present in the nonataxic A1 founder (Table 1). We were unable to study ventral horn neurons of the founders since we had not preserved their spinal cords. A comparison of spinal cord expression in the D2 and D11 lines, however, revealed high transgene expression in D2 and low expression in D11, even though both lines exhibited severe ataxia (Table 1). Thus, of all the transgene-expressing neurons, levels in the DCN tracked most closely with disease severity.

Two additional factors argue against a significant contribution by noncerebellar transgene-expressing neurons to the cerebellar ataxic phenotype. First, neocortical layer V neurons, brain stem nuclei (red, pontine, hypoglossal, gigantocellular), and ventral horn neurons of the spinal cord have never been implicated in cerebellar ataxia. Second, lesions in each of these nuclei produce a characteristic set of clinical features, none of which are observed in the Tg mice. Lesions of neocortical layer V neurons or increased drive of ventral horn spinal neurons are accompanied by increased muscle tone, spasticity, and postural abnormalities, while impaired function

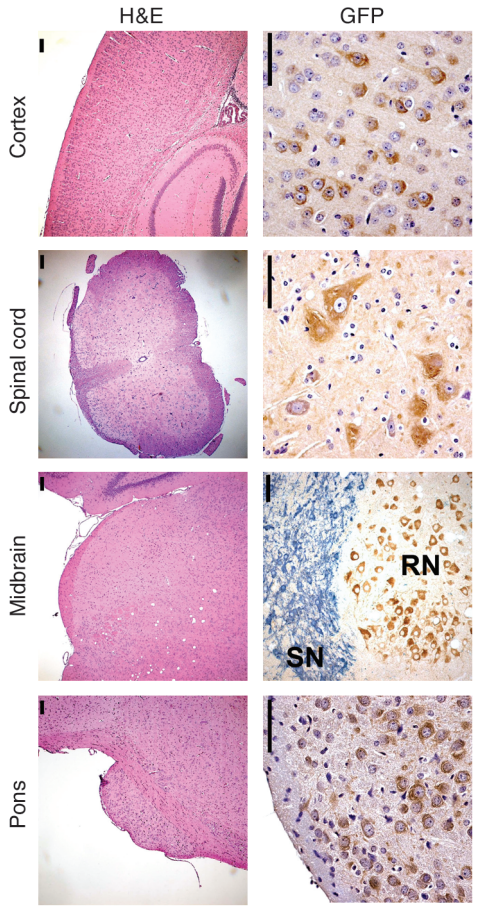

Figure 4
Transgene expression in different regions of the brain. H&E staining (left) and transgene expression (right) in the layer V neocortex, spinal cord anterior horn cells, red nucleus, and pontine nucleus (brown). In the midbrain section tyrosine hydroxylase–positive neurons appear blue. SN, substantia nigra, RN, red nucleus. Scale bars = 100 μm.

of spinal neurons results in lower motor neuron paralysis (22), features not seen in the Tg model. Isolated lesions in the red nucleus do not cause overt gait ataxia (23), but degeneration of the red nucleus in combination with the inferior olivary nucleus and cerebellar Purkinje neurons cause wasted thigh muscles, lower motor neuron impairment, and thoracic kyphoscoliosis (24), none of which was seen in our model. Isolated pontine degeneration has been reported to cause quadriplegia and pseudobulbar palsy (25), neither of which was exhibited by the Tg mice. These reasons, along with the data presented in Table 1, suggest that a direct and/or substantial contribution to the major cerebellar phenotype by transgene-expressing noncerebellar neurons is unlikely. These noncerebellar transgene-expressing neurons receive projections from the DCN (cerebello-rubral, cerebello-thalamic, cerebello-vestibular, and cerebello-reticular pathways), however, and they may therefore indirectly modify the phenotype (3, 26). The absence of neurodegeneration suggests that an electrical alteration in the DCN, the only neurons in the cerebellum expressing the transgene, is the predominant cause of the observed cerebellar ataxia.

DCN hyperexcitability due to SK channel suppression and loss of I_{AHP}. We focused on the electrical properties of DCN, since ataxia in these Tg mice is likely to be predominantly of cerebellar origin, and transgene expression within the cerebellum is restricted to the DCN. Enhanced neuronal excitability has been reported to follow pharmacological blockade by apamin of SK channels that underlie a component of the I_{AHP} (7, 10, 27, 28). Immunohistochemistry studies with SK isoform-specific Ab's (18) revealed SK2 and SK1 (Figure 6a), but not SK3 protein (not shown) in DCN neurons. SK3-1B-GFP has been previously demonstrated to selectively suppress SK1 and SK2 channels without affecting voltage-gated K^+ currents in heterologous mammalian expression systems (12), and such dominant-inhibitory activity in Tg DCN neurons would, like apamin, cause DCN hyperexcitability.

Whole-cell slice recordings using an established protocol for SK channels (10) revealed a prominent I_{AHP} in non-Tg DCN neurons (Figure 6b, $n = 20$), which was completely inhibited by apamin, a selective SK channel blocker (Figure 6c, $n = 6$). Tg DCN neurons showed a significant reduction in I_{AHP} amplitude comparable to apamin-treated non-Tg neurons (Figure 6d, $n = 32$). The summarized data in Figure 6e demonstrate a greater than tenfold decrease in I_{AHP} amplitude in Tg

Table 1
Tabulation of transgene expression levels in D2 and D11 lines and other founder Tg mice

Founder	Cerebellar ataxia	Cerebellar cortex	DCN	Red nucleus	Pontine nucleus	Motor cortex	Spinal cord
D2	Severe	–	+++	+++	+++	+	+++
D11	Severe	–	+++	+++	+++	++	+
F5	Severe	–	+++	+++	++	++	NT
D9	Severe	–	+++	+++	++	++	NT
A2	Mild	–	+	+++	–	–	NT
F4	Mild	–	+	+	–	–	NT
B3	–	–	–	–	–	+	NT
A1	–	–	–	+	–	–	NT

Summary of the expression profile in Tg mice. NT, not tested.

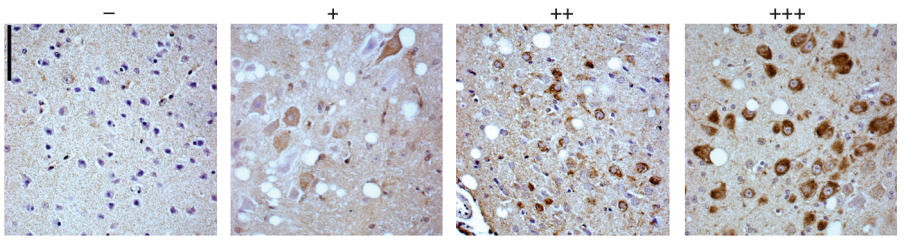

Figure 5
Grading scheme for transgene expression levels. Examples of sections immunostained for GFP showing relative expression levels and corresponding grade from – to +++. Scale bar = 100 μm.

and apamin-treated non-Tg DCN neurons compared with non-Tg controls ($P < 0.001$ between controls and apamin-treated non-Tg or Tg neurons) due to transgene-mediated SK channel suppression.

Thirty percent of DCN neurons exhibited rhythmic spontaneous firing under our recording conditions. The firing frequency of non-Tg DCN neurons was 6.3 Hz (Figure 6f, $n = 6$). Consistent with the loss of the I_{AHP}, Tg neurons (Figure 6h, $n = 8$) and apamin-treated non-Tg neurons (Figure 6g, $n = 3$) lacked the after-hyperpolarization and exhibited a spontaneous firing frequency more than double that of non-Tg neurons (summarized in Figure 6i, left). There was an apparent shift in the resting membrane potential in voltage traces of both Tg neurons and apamin-treated non-Tg neurons. The true resting potential of these neurons was difficult to determine due to their fast spiking (8), however, and thus apparent elevation of the resting potential is probably a consequence of loss of the after-hyperpolarization and increased spiking rather than true changes in resting membrane conductance.

A generalized nonspecific effect by the transgene on DCN function can be excluded because other electrogenic processes are intact in Tg DCN neurons. Spike duration (Figure 6i, right) and voltage-gated Ca^{2+} and other K^+ current amplitudes (Figures 7, a and b) are similar in Tg and non-Tg DCN neurons, indicating that other conductances in Tg DCN neurons are unaffected. We considered the possibility that the altered electrical and motor phenotype could result from gross disturbances of CaM homeostasis in addition to I_{AHP} suppression because the transgene retains the CaM-binding domain of SK channels (11, 12). The CaM-mediated Ca^{2+} current inactivation (29) (Figure 7, c and d) is similar in Tg and non-Tg DCN neurons, however, suggesting that other CaM-mediated events are not altered in Tg neurons and that SK3-1B-GFP is not acting as a "CaM sponge." Furthermore, the CaM antagonist trifluoperazine has never been reported to cause cerebellar ataxia despite extensive clinical use (30). These observations, taken together with the absence of neurodegeneration in any CNS region (Figures 4 and 5), indi-

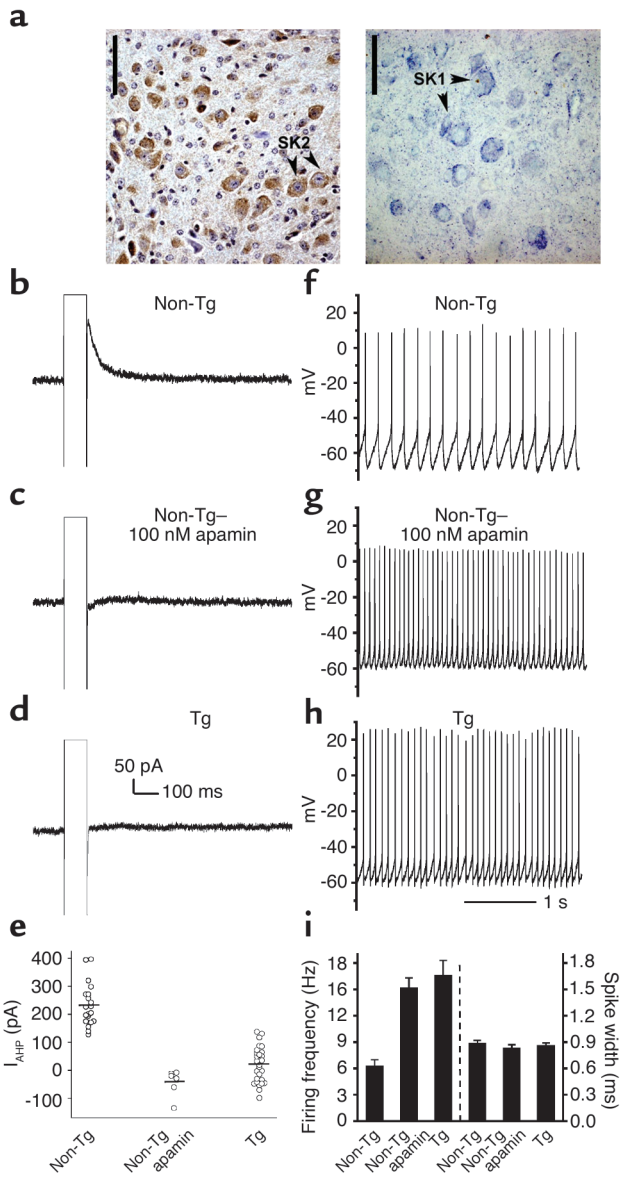

Figure 6
Transgene-expressing DCN neurons are hyperexcitable. (**a**) DCN neurons express SK2 (indicated by arrowheads pointing to brown SK2 cells) and SK1 (arrowheads points to blue SK1 cells). SK3 was detected in the midbrain but not in the DCN (not shown). Scale bars = 100 μm. (**b**) I_{AHP} in non-Tg DCN. (**c**) I_{AHP} in non-Tg DCN is apamin-sensitive. (**d**) I_{AHP} is absent from Tg DCN. (**e**) I_{AHP} amplitude data summarized. (**f**) Non-Tg DCN neurons fire spontaneously at approximately 6.3 Hz and exhibit a prominent post-spike after-hyperpolarization. (**g**) Non-Tg DCN exposed to 100 nM apamin fire more rapidly at approximately 15.2 Hz and do not show the after-hyperpolarization. (**h**) Tg DCN fire spontaneously at approximately 16.6 Hz and lack the after-hyperpolarization. (**i**) Summary of mean firing frequency (left) and spike width measured at half amplitude (right). Error bars = SEM.

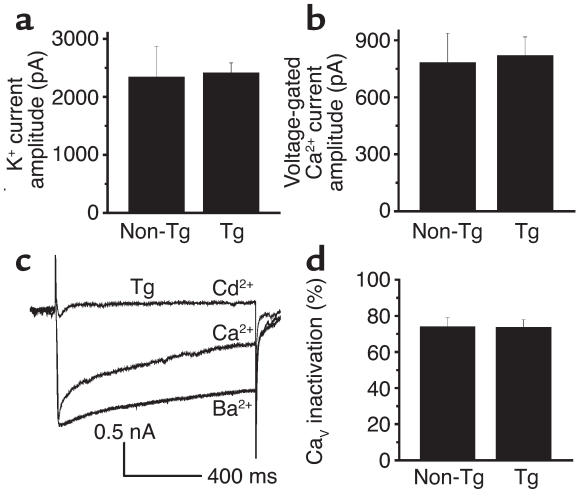

Figure 7
Other conductances in Tg neurons are unaffected. (**a**) Amplitude of apamin-resistant K^+ currents in non-Tg and Tg DCN neurons (n = 6 non-Tg, 32 Tg). (**b**) Peak voltage-gated Ca^{2+} currents in Tg and non-Tg DCN neurons. (**c**) Ca^{2+} currents in Tg DCN neurons demonstrating Ca^{2+}-CaM–dependent but not Ba^{2+}-dependent current inactivation. The Ba^{2+} trace is scaled to the peak amplitude of the Ca^{2+} trace (**d**). Ca^{2+} current inactivation summarized (n = 5 non-Tg, 8 Tg; $P > 0.05$). Ca_V, voltage-gated CA^{2+}. Error bars = SEM.

cate that SK3-1B-GFP causes DCN hyperexcitability by selectively suppressing SK1 and SK2 channels, a process coincident with the onset of cerebellar ataxia.

Discussion

Cerebellar ataxia may in part be initiated as a consequence of increased DCN excitability secondary to loss of inhibitory input from Purkinje neurons that frequently degenerate or are functionally altered in this disease (3). This mechanism of disease initiation predicts that intrinsic DCN hyperexcitability in the absence of upstream alterations in Purkinje inhibitory input would cause cerebellar ataxia. We have tested this mechanism by using a family-wide dominant-negative strategy to selectively silence SK channels, regulators of excitability, in DCN neurons in Tg mice. These mice developed characteristic features of cerebellar ataxia including severe incoordination, postural instability, gait ataxia, and intention tremor, without rigidity, muscle wasting, or sensory deficits. The phenotype was evident on postnatal day 11, progressed until about 3 weeks, and was relatively unchanged thereafter. Development of cerebellar ataxia was coincident with transgene expression in DCN neurons, and no expression was seen elsewhere in the cerebellum. The transgene product was also observed in the motor strip, brain stem nuclei (red, pontine, hypoglossal, gigantocellular), and ventral horn neurons of the spinal cord, but expression levels in these areas did not correlate with disease severity. Furthermore, these regions have never been implicated in cerebellar ataxia, and the clinical features associated with dysfunction in these nuclei were not present in our Tg model (22–25). No signs of neurodegeneration were evident in any region of the central nervous system until 6 months of age (the longest time examined). Slice recordings revealed suppression of I_{AHP}, loss of the after-hyperpolarization, and a doubling of firing frequency in Tg DCN neurons compared with non-Tg neurons, indicative of enhanced DCN excitability. Other electrogenic conductances in these neurons were unaffected. This Tg model demonstrates that intrinsic DCN hyperexcitability due to selective suppression of SK channels in the absence of neurodegeneration is sufficient to induce severe cerebellar ataxia.

Other ataxic models have varying severity of ataxia that often does not correlate with the severity of the lesion (3). This is believed to be due to secondary degenerative and compensatory mechanisms as well as neuronal reactions in the DCN. A postulated compensatory mechanism in these models is enhancement of intranuclear inhibition by inhibitory interneurons within the DCN. By directly increasing excitability in the large neurons in the DCN that are glutamatergic projection neurons (21), our model may preempt the development of inhibitory compensatory mechanisms, thus explaining the severe ataxia that is observed.

There is some doubt as to the role of SK channels in regulating firing in DCN neurons. In our experiments, pharmacological blockade of SK channels in non-Tg DCN neurons with apamin or genetic suppression of these channels in Tg neurons with the dominant-negative SK3-1B-GFP caused a significant increase in firing frequency similar to what has been described in DCN and vestibular neurons (7, 28). We did not observe "bursting behavior," however, in contrast to an earlier slice study that reported such activity in DCN neurons following SK channel blockade (7). Our results and those from other slice studies differ from those in a report that SK channel inhibitors have minimal effects on firing frequency in dissociated DCN neurons (8). These differences may stem from details of the preparation (slice versus dissociated neurons), temperature, and/or Ca^{2+} buffering power of the pipette solutions; high concentrations of Ca^{2+} buffers have been shown to suppress the development of SK currents (10). In balance, our studies in conjunction with previous slice studies highlight the important contribution of SK channels to the regulation of DCN firing frequency and suggest a role for SK channels in the pathogenesis of ataxia. SK3 knockout mice do not exhibit an overt neurological phenotype (31), possibly due to compensation by other SK channels. In contrast, our powerful family-wide dominant-negative approach successfully induced a neurological phenotype and may be extended to other neuronal pathways and to nonneuronal tissues through the use of region- and tissue-specific promoters to further define the in vivo role of SK channels.

In conclusion, cerebellar ataxia can be induced in Tg mice by hyperexcitability of DCN neurons in the absence of cerebellar degeneration, although modifying contributions from other Tg-expressing motor nuclei cannot be completely ruled out. Degenerating Purkinje neurons in other ataxia models could elicit retrograde reactions in cerebellar inputs, while in our model Purkinje neurons are intact, and DCN hyperexcitability is likely to be the predominant cause of the observed cerebellar ataxia. In some forms of human cerebellar ataxia, hyperexcitability in DCN neurons and other target motor nuclei secondary to loss of Purkinje inhibitory input may represent a critical step in the manifestation of the disease. Since SK channels are critical regulators of firing, our observations raise the possibility that SK openers such as the FDA-approved neuroprotective agent riluzole (32) may reduce neuronal hyperexcitability and thereby therapeutically benefit cerebellar ataxia.

Acknowledgments

This work was supported by grants from the National Ataxia Foundation (K.G. Chandy), the NIH (K.G. Chandy and F.M. LaFerla), the March of Dimes (M.E. Barish), the Juvenile Diabetes Research Foundation (K.G. Chandy), and the Austrian Science Foundation (H.G. Knaus). V.G. Shakkottai was supported by a predoctoral fellowship from the American Heart Association Western States Affiliate. We thank Michael D. Cahalan, J. Jay Gargus, Rui-lin Wu, Diane K. O'Dowd, Stephan Grissmer, Todd C. Holmes, Aaron Kolski-Andreaco, Heike Wulff, and John Adelman for helpful discussions and suggestions.

1. Rosenberg, R.N. 1995. The genetic basis of ataxia. *Clin. Neurosci.* **3**:1–4.
2. Klockgether, T., and Dichgans, J. 1997. The genetic basis of hereditary ataxia. *Prog. Brain Res.* **114**:569–576.
3. Grusser-Cornehls, U., and Baurle, J. 2001. Mutant mice as a model for cerebellar ataxia. *Prog. Neurobiol.* **63**:489–540.
4. Trouillas, P., et al. 1997. International Cooperative Ataxia Rating Scale for pharmacological assessment of the cerebellar syndrome. The Ataxia Neuropharmacology Committee of the World Federation of Neurology. *J. Neurol. Sci.* **145**:205–211.
5. Figueroa, K.P., et al. 2001. Association of moderate polyglutamine tract expansions in the slow calcium-activated potassium channel type 3 with ataxia. *Arch. Neurol.* **58**:1649–1653.
6. Sotelo, C., and Alvarado-Mallart, R.M. 1991. The reconstruction of cerebellar circuits. *Trends Neurosci.* **14**:350–355.
7. Aizenman, C.D., and Linden, D.J. 1999. Regulation of the rebound depolarization and spontaneous firing patterns of deep nuclear neurons in slices of rat cerebellum. *J. Neurophysiol.* **82**:1697–1709.
8. Raman, I.M., Gustafson, A.E., and Padgett, D. 2000. Ionic currents and spontaneous firing in neurons isolated from the cerebellar nuclei. *J. Neurosci.* **20**:9004–9016.
9. Telgkamp, P., and Raman, I.M. 2002. Depression of inhibitory synaptic transmission between Purkinje cells and neurons of the cerebellar nuclei. *J. Neurosci.* **22**:8447–8457.
10. Faber, E.S., and Sah, P. 2002. Physiological role of calcium-activated potassium currents in the rat lateral amygdala. *J. Neurosci.* **22**:1618–1628.
11. Xia, X.M., et al. 1998. Mechanism of calcium gating in small-conductance calcium-activated potassium channels. *Nature.* **395**:503–507.
12. Tomita, H., et al. 2003. Novel truncated isoform of SK3 potassium channel is a potent dominant-negative regulator of SK currents: implications in schizophrenia. *Mol. Psychiatry.* **8**:524–535.
13. Oddo, S., et al. 2003. Triple-transgenic model of Alzheimer's disease with plaques and tangles: intracellular Abeta and synaptic dysfunction. *Neuron.* **39**:409–421.
14. Caroni, P. 1997. Overexpression of growth-associated proteins in the neurons of adult transgenic mice. *J. Neurosci. Methods.* **71**:3–9.
15. Feng, G., et al. 2000. Imaging neuronal subsets in transgenic mice expressing multiple spectral variants of GFP. *Neuron.* **28**:41–51.
16. Crawley, J.N. 2000. *What's wrong with my mouse?* Wiley-Liss. New York, New York, USA. 329 pp.
17. Barlow, C., et al. 1996. Atm-deficient mice: a paradigm of ataxia telangiectasia. *Cell.* **86**:159–171.
18. Sailer, C.A., et al. 2002. Regional differences in distribution and functional expression of small-conductance Ca^{2+}-activated K^+ channels in rat brain. *J. Neurosci.* **22**:9698–9707.
19. Schmued, L.C., and Hopkins, K.J. 2000. Fluoro-jade B: a high affinity fluorescent marker for the localization of neuronal degeneration. *Brain Res.* **874**:123–130.
20. Zeilhofer, H.U., Blank, N.M., Neuhuber, W.L., and Swandulla, D. 2000. Calcium-dependent inactivation of neuronal calcium channel currents is independent of calcineurin. *Neuroscience.* **95**:235–241.
21. Sultan, F., Konig, T., Mock, M., and Their, P. 2002. Quantitative organization of neurotransmitters in the deep cerebellar nuclei of the Lurcher mutant. *J. Comp. Neurol.* **452**:311–323.
22. Wilson, J.D., et al. 1991. *Harrison's principles of internal medicine.* 12th edition. McGraw Hill. New York, New York, USA. 158–160.
23. Muir, G.D., and Whishaw, I.Q. 2000. Red nucleus lesions impair overground locomotion in rats: a kinetic analysis *Eur. J. Neurosci.* **12**:1113–1122.
24. Guyer, C.L., et al. 2002. A line of Berlin Druckrey IV rats proposed as a new model for human hereditary ataxia. *In Vivo.* **16**:255–263.
25. Stein, J.H. 1990. *Internal medicine.* 3rd edition. Little, Brown and Company Inc. Boston, Massachusetts, USA. 2033 pp.
26. Tarnecki, R., Lupa, K., and Niechaj, A. 2001. Responses of the red nucleus neurons to stimulation of the paw pads of forelimbs before and after cerebellar lesions. *J. Physiol. Pharmacol.* **52**:423–436.
27. Cingolani, L.A., Gymnopoulos, M., Boccaccio, A., Stocker, M., and Pedarzani, P. 2002. Developmental regulation of small-conductance Ca^{2+}-activated K^+ channel expression and function in rat Purkinje neurons. *J. Neurosci.* **22**:4456–4467.
28. Smith, M.R., Nelson, A.B., and Du Lac, S. 2002. Regulation of firing response gain by calcium-dependent mechanisms in vestibular nucleus neurons. *J. Neurophysiol.* **87**:2031–2042.
29. Erickson, M.G., Liang, H., Mori, M.X., and Yue, D.T. 2003. FRET two-hybrid mapping reveals function and location of L-type Ca^{2+} channel CaM preassociation. *Neuron.* **39**:97–107.
30. Gilman, A.G., Rall, T.W., Nies, A.S., and Taylor, P. 1990. *Goodman and Gilman's the pharmacological basis of therapeutics.* 8th edition. Pergamon Press. New York, New York, USA. 383–435.
31. Bond, C.T., et al. 2000. Respiration and parturition affected by conditional over-expression of the Ca^{2+}-activated K^+ channel subunit, SK3. *Science.* **289**:1942–1946.
32. Cao, Y.J., Dreixler, J.C., Couey, J.J., and Houamed, K.M. 2002. Modulation of recombinant and native neuronal SK channels by the neuroprotective drug riluzole. *Eur. J. Pharmacol.* **449**:47–54.